ELSEVIER

Atmospheric Environment 38 (2004) 6655–6665

ATMOSPHERIC ENVIRONMENT

www.elsevier.com/locate/atmosenv

Evolution of particle number distribution near roadways. Part II: the 'Road-to-Ambient' process

K. Max Zhang[a], Anthony S. Wexler[a,b,c,*], Yi Fang Zhu[d], William C. Hinds[d], Constantinos Sioutas[e]

[a]*Department of Mechanical and Aeronautical Engineering, University of California, Davis, CA 95616, USA*
[b]*Department of Civil and Environmental Engineering, University of California, Davis, CA 95616, USA*
[c]*Department of Land, Air, and Water Resources, University of California, Davis, CA 95616, USA*
[d]*Department of Environmental Health Sciences, University of California Los Angeles, 650 Charles E. Young Drive South, Los Angeles, CA 90095, USA*
[e]*Department of Civil and Environmental Engineering, University of Southern California, 3620 South Vermont Avenue, Los Angeles, CA 90089, USA*

Received 19 December 2003; received in revised form 17 June 2004; accepted 24 June 2004

Abstract

The 'road-to-ambient' evolution of particle number distributions near the 405 and 710 freeways in Los Angeles, California, in both summer and winter, were analyzed and then simulated by a multi-component sectional aerosol dynamic model. Condensation/evaporation and dilution were demonstrated to be the major mechanisms in altering aerosol size distribution, while coagulation and deposition play minor roles. Seasonal effects were significant with winters generally less dynamic than summers. A large number of particles grew into the >10 nm range around 30–90 m downwind of the freeways. Beyond 90 m some shrink to <10 nm range and some continued growing to >100 nm as a result of competition between partial pressure and vapor pressure. Particle compositions probably change dramatically as components adapt to decreasing gas-phase concentration due to dilution, so number distribution evolution is also an evolution of composition. As a result, people who live within about 90 m of roadways are exposed to particle sizes and compositions that others are not.

Keywords: Ultrafine particles; Freeways; Size distribution; Aerosol model; Air quality

1. Introduction

Nationally transportation is responsible for more than 50 percent of carbon monoxide, about 34 percent of nitrogen oxide (NO_x) emissions, more than 29 percent of hydrocarbon emissions and as much as 10 percent of fine particulate matter emissions (STPP, 2003). In metropolitan areas, such as Southern California, transportation is the dominant emission source. Epidemiological studies have linked air pollution to a host of serious public health concerns including asthma, cancer, heart disease, strokes, high blood pressure, birth defects, and brain damage (STPP, 2003). The Children's Health Study (CHS), one of the largest and most comprehensive

*Corresponding author. Department of Mechanical and Aeronautical Engineering, University of California, Davis, CA 95616, USA. Tel.: +1-530-754-6558; fax: +1-530-752-4158.

E-mail address: aswexler@ucdavis.edu (A.S. Wexler).

1352-2310/$ - see front matter © 2004 Elsevier Ltd. All rights reserved.
doi:10.1016/j.atmosenv.2004.06.044

investigations of the long-term consequences of air pollution on the respiratory health of children, found that lung function growth was approximately 10 percent slower among children living in communities with higher level of traffic-related pollutants (Kunzli et al., 2003). In a cohort of 5000 adults followed up for 8 years, cardiopulmonary mortality was found to be associated with living near a major road and, less consistently, with the estimated ambient background concentration (Hoek et al., 2002). A study conducted by the South Coast Air Quality Management District found that the additional cancer risk along highway corridors with significant big truck traffic was higher than anywhere else in the Los Angeles region, and much higher than the regional average of 1200–1400 per million residents (SCAQMD, 2000). Those studies make cutting mobile emissions imperative to protect public health.

Since mobile emission control could also involve large economic and social consequences, decision makers need scientific tools to adopt optimal control strategies. In Part I of this series (Zhang and Wexler, 2004), we analyzed the aerosol dynamics near roadways and proposed a structure for a mechanistic roadway air quality model that provides a tool for evaluating the impact of transportation on ambient air quality and serves as a 'plume-in-grid' model for mobile sources (Zhang and Wexler, 2004). The model consists of two sub-modules, 'tailpipe-to-road' and 'road-to-ambient'. In the 'tailpipe-to-road' process, the important processes include turbulence mixing by moving traffic, nucleation and condensation. In the 'road-to-ambient' process, dilution and condensation are dominant. Coagulation in both processes is too slow compared to the dilution scale to be important (Zhang and Wexler, 2004).

Here we analyzed data collected near the 405 and 710 freeways in Los Angeles, CA (Zhu et al., 2002a, b) and simulate the dynamics. The paper is organized as follows: First we analyze the data sets based on our understanding of aerosol dynamics in the 'road-to-ambient' process; then we introduce a multi-component aerosol dynamic model and its simulation results; finally we discuss the implications of the analysis and simulation and point out the direction for further studies.

2. Data analysis

2.1. Data collection

Particle number concentrations and size distributions in the size range from 6 to 220 nm, CO and black carbon concentrations as well as meteorological data were measured at various distances downwind and upwind near two major freeways in Los Angeles, CA, 405 and 710, in both summer and winter seasons (Zhu et al., 2002a, b, 2004). Hereafter we refer to them as 405S (i.e., summer study near Highway 405), 405W, 710S and 710W. Table 1 summarizes the sampling dates and sites. At each sampling position, three samples (called passes) for each measurement were taken in sequence (Zhu et al., 2002a).

2.2. Conservation of number

Zhang and Wexler (2002a) analyzed the effects of different aerosol processes on number distributions for an aerosol population: Condensation/evaporation only change particles size, while preserving its total number; coagulation works mainly to decrease the number of small particles and has negligible effect on larger ones; deposition removes particles from the atmosphere and nucleation creates new particles. As discussed in Part I (Zhang and Wexler, 2004), dilution and condensation/evaporation are the dominant mechanisms changing aerosol number distribution in the 'road-to-ambient' process, while coagulation and deposition play minor roles. Since the particle number concentration can only be changed by dilution, if we follow an air parcel advecting from the roadway, its total number of particles should be conserved after dilution is taken into account. However, atmospheric particles vary in size from 1 to 10 μm, of which the measurements only covered a fraction, i.e., 6–220 nm. Let us regard an air parcel as a particle size bounded (6–220 nm) control volume, which constantly exchanges particles with outside—particles smaller than 6 nm may grow or particles larger than 220 nm may shrink into this volume and similarly, particles within the volume may shrink or grow out. All of the above pose uncertainties for the data analysis.

Table 1
Dates and locations of the field campaign

Study	Date	Location	Sampling distances downwind (m)
405S	05/15–07/18/2001	The Los Angeles National Cemetery adjacent to Interstate 405	30, 60, 90, 150, 300
405W	01/11–01/20/2002		
710S	08/30–10/27/2001	City of Downey along Southern Avenue	17, 20, 30, 90, 150, 300
710W	01/14–01/25/2002		

The exchanges at the lower and upper end of the control volume possess different characteristics. At the upper end, (1) the particles larger than 200 nm have very low number concentration measured and (2) the growth time scale for those particles is much slower than the dilution time scale (Zhang and Wexler, 2004), which implies that movement across the upper boundary is negligible. In contrast, at the lower end, small particles initially grow very fast and exert a strong influx on the control volume. But their growth rates will decrease as they grow (Zhang and Wexler, 2002a) and as the ambient concentrations of condensable materials are diluted by ambient air. So there exists a group of particles whose distribution is not influenced by the exchanges in the lower end and only slightly by exchanges in the upper end. Therefore, the total number concentration in that group is conserved after dilution is taken into account.

2.3. Modal shapes

The measured size distributions also showed pronounced modes (Zhu et al., 2002a), which could be used to track particle growth behavior. For example, the distribution measured 30 m downwind on June 20, 2001 at 405S is clearly composed of three or four modes (Fig. 1): A large mode around 7–20 nm (M30A), a small mode around 50–200 nm (M30C) and between 20 and 50 nm there were one or two other modes (M30B). At 60 m, the profile showed a small mode around 8–20 nm (M60A) and a large mode around 20–100 nm (M60B). Within mode M60B there could be two or three smaller modes. At 90 m, modes around 20–30 nm (M90A) and 30–100 nm (M90B) were evident. There was also a tail below 8 nm at 60 and 90 m (M60T and M90T). Since sub-10 nm measurements were achieved with the SMPS by increasing sampling flow rate, M60T and M90T are

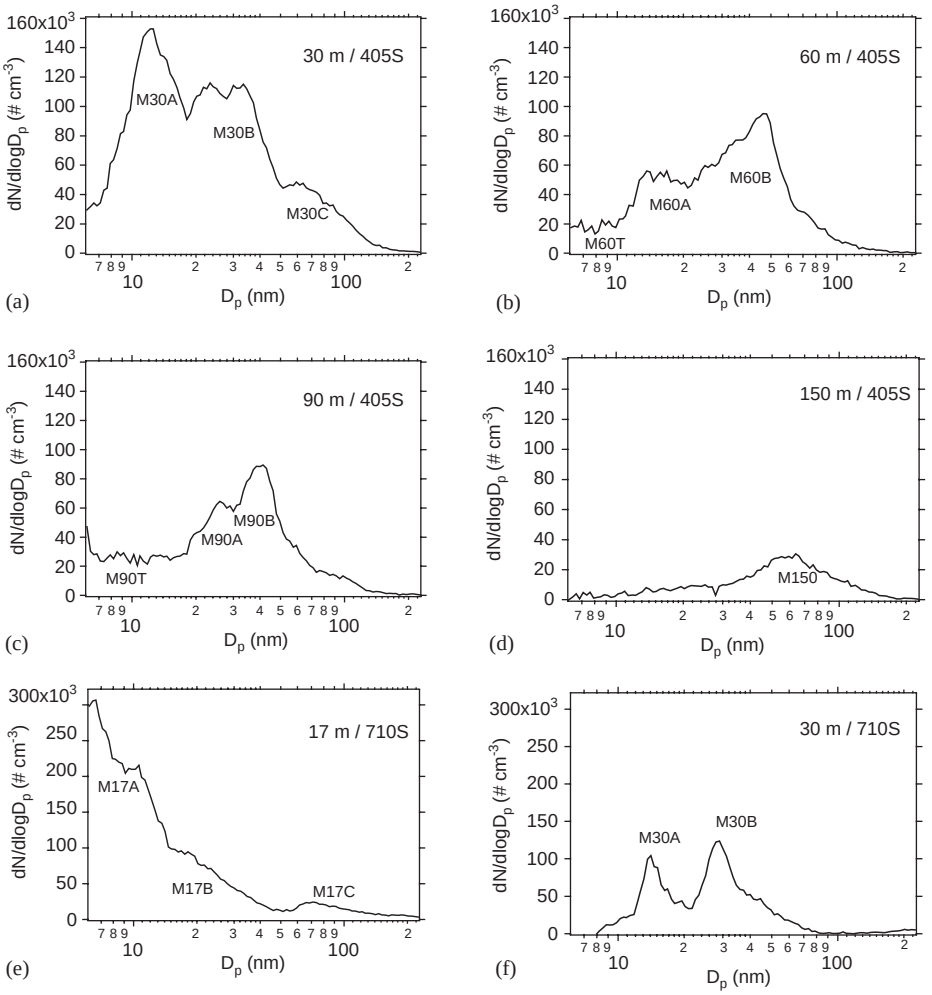

Fig. 1. The measured number distribution profiles had clear modal shapes like those collected in Highway 405 and 710 summer study (405S and 710S): (a) 405S at 30 m, (b) 405S at 60 m, (c) 405S at 90 m, (d) 405S at 150 m, (e) 710S at 17 m, (f) 710S at 30 m.

associated with large uncertainty. At 150 and 300 m, there was only one recognizable mode (M150 and M300, respectively). But the diameter corresponding to the peak of M300 (80 nm) was larger than that of M150 (60 nm), a clear indication of particle growth from 150 to 300 nm.

2.4. Using CO as the dilution indicator

We have already derived the dilution equation in Part I (Zhang and Wexler, 2004). Assuming that exhaust and upwind concentration does not change with time and making a little manipulation, we have

$$\frac{n(D_p, t+\Delta t) - n_B(D_p)}{n(D_p, t) - n_B(D_p)} = \frac{f(t+\Delta t)}{f(t)} = \frac{C(t+\Delta t) - C_B}{C(t) - C_B}, \quad (1)$$

where C and C_B are concentration and upwind concentration of non-reactive gas, which can serve as a dilution indicator. Eq. (1) holds under the reasonable assumption that both particles and gases dilute in the same way. Although both CO and black carbon (BC) were measured in the field campaign, dilution ratios derived from each were inconsistent (Zhu et al., 2002a). CO was used solely as indicator of dilution ratio in this study, because it is more reliably measured than BC. Since CO concentrations were measured at various distances, f became a function of distance, x, instead of time, t, so $f(x)/f(x+\Delta x)$ indicated the dilution ratio between x and $x+\Delta x$, and is called the stepwise dilution ratio in Table 2. In spite of its obvious advantages, using CO or any other gases as dilution indicators has a fundamental drawback in that its value becomes highly uncertain as its concentration approaches either ambient values or the instrument detection limit. In our study, dilution ratios from 150 to 300 m suffer such weakness.

2.5. Analysis of 405S data

The number distribution profiles measured in 405S study were very stable. Not only did all three passes in the same day agree very well, but also the distributions measured during adjacent days were very close, implying that traffic composition and meteorological conditions were very stable during the measuring period.

We start with M150, which had a number concentration of 15,513 cm^{-3}. If the total number concentration of this mode was conserved, it would have been about 25,900 cm^{-3} at 90 m, i.e., taking into account a dilution of $f(90)/f(150) = 1.67$. That was nearly equal to the number concentrations of particles from 30 to 220 nm (25,397 cm^{-3}), where M90B was located. Following the same thought, a dilution-adjusted concentration of 38,000 cm^{-3} was similar to that of M60B (20–220 nm; 39,074 cm^{-3}). At 30 m, that concentration would have been 102,960 cm^{-3}, which was equal to the concentration of total particles measured, i.e., sum of M30A, M30B and M30C (103,556 cm^{-3}). So both qualitatively and quantitatively, a group of particles, ranging from 6 to 220 nm in size at 30 m, stayed in the control volume from 30 to 150 m. Do M60A and M90A have any relation? M90A has a concentration of 10,385 cm^{-3}, which gave a dilution-adjusted concentration at 60 m of 15,266 cm^{-3}. That was very close to the concentration of M60A (15,269 cm^{-3}). If we take a close look at the process from 30 to 60 m, M30A corresponded to particles from 20 to 40 nm and M30B together with M30C matched particles from 40 to 220 nm. Finally, we diluted M150A with the factor listed in Table 2, which gave about 6890 cm^{-3}, much larger than the total number concentration (6–220 nm) at 300 m. However, the uncertainties associated with CO measurement at 300 m were significant. In order to verify the viability of this analysis, the 405S data collected on the other two days with concurrent CO measurement available was also examined. They all followed a similar pattern.

Through the analysis above we gained valuable insights into the aerosol dynamics during this evolution process. From 30 to 60 m, particles in M30A grew into the 20–40 nm range. The peak we observed between 40 and 60 nm contained a fraction of M30C, which shrank to smaller size, and most of M30B. New particles, originally outside of the system, grew into it and formed a mode, i.e., M60A. From 60 to 90 m, some particles in M60B grew modestly and some shrank. The M60A

Table 2
The stepwise dilution ratio determined by measured CO concentration

Sampling distance (m)	Conc.[a] (ppm)	Dilution ratio
405S		
30	2.03	N/A
60	0.83	2.64
90	0.60	1.47
150	0.40	1.67
300	0.23	2.25
405W		
30	2.03	N/A
60	1.23	1.71
90	1.07	1.17
150	0.70	1.61
300	0.40	2.00
710S		
17	2.43	N/A
30	1.33	1.89
150	0.40	4.11
300	0.20	3.00

[a]Reported CO concentrations are background subtracted.

continued growing to 20–30 nm. A new burst of particles outside the range, M60T and M90T, started to grow into the system. But they did not manage to grow large enough to stay in the system. Neither did M90A, known at 60 m as M60A. At 150 m they disappeared. From 90 to 150 m, some of M90C shank and some grew, which broadened the size spectrum from 30–220 to 10–220 m. As discussed earlier, we are not so certain about the 150–300 m process, but qualitatively the 90–150 m trend appears to continue.

2.6. Analysis of 405W data

Comparing to 405S, 405W saw predominantly fractions of small particles (<30 nm) in the size distribution profiles. Both the 30–60 m process and the 60–90 m process saw shrinking of particles in all size ranges. The 90–150 m process resembled the 405S: Some particle grew and some shrank, making the mode broader. Compared to 405S, the shapes of size distributions of 405W were generally preserved, indicating that winter was less dynamic than summer. This seasonal effect can also be perceived by comparing 710S and 710W.

2.7. Analysis of 710S data

The number distribution profiles measured at the 710S varied a lot from pass to pass and day to day. This was probably due to the traffic mix on the 710 consisting of about 25 percent diesel and 75 percent gasoline-powered vehicles. A more varied traffic composition makes emission more time-dependent, while a more uniform traffic composition in 405S makes emission less time-dependent. Counter-intuitively, number concentrations lower than upwind values were commonly observed and CO concentrations measured at 90 m were systematically lower than those at 150 m. So the uncertainties for the 710S were significantly larger than the 405S. In addition, the first and second sampling location, 17 and 20 m, were so close to each other that aerosol dynamics analysis was difficult. Considering all these factors, we focused on the 17–30, 30–150 and 150–300 m processes at the 710S.

In spite of those uncertainties, an aerosol dynamic pattern similar to 405S was identified. The size distribution at 17 m was composed of 3 modes: M17A (6–10 nm), M17B (10–50 nm) and M17C (50–220 nm). M17B may consist of two sub-modes, one from 10 to 12 nm and the other from 12 to 50 nm. From 17 to 30 m, most of particles in M17B grew into the 20–100 nm size range, while particles in M17C shrank into that range. Together they formed M30B. A fraction of M17A grew into M30A (10–20 nm) but then evaporated out of the measurement range at 150 m. M30B continued growing, making M150 at 150 m. Again, the modal size range broadened from 150 to 300 m with some particles growing to larger size.

2.8. Analysis of 710W data

710W data suffer the similar sporadic error as 710S—20–40 percent differences between passes were commonly observed in all size ranges. On the other hand, the size distributions were very stable with two modes persisting from 17 to 300 m. Taking those uncertainties into account, dilution-only can explain the evolution process except at the very beginning, from 17 to 30 m, where small particles grew into the system and original particles in the systems grew to larger size.

3. Model description

3.1. Evolution of aerosol number distribution was a dynamic process

Engine exhaust is a complex mixture. During the tailpipe-to-road process, the sharp drop in temperature and relatively high concentrations lead to significant condensation of vapor emissions, making particle composition a complex mixture, too. The relative amount of condensed materials usually depends on particle size. As exhaust disperses from roadways, the gas-phase concentration decreases. Then during the road-to-ambient process, some compounds may continue condensing while others may begin evaporating, depending on the relative magnitude of their partial and vapor pressure. In addition, the vapor pressure is further modified by the molar fraction of each component in the particle phase according to Raoult's law and by the Kelvin effect, which has profound impact on the dynamics of small particles (Zhang and Wexler, 2002a). This competition between partial pressure and Raoult- and Kelvin-adjusted vapor pressure coupled with dilution is the main reason why some particles grew and others shrank at the same time. Volatile gases may evaporate from particles to achieve gas–particle equilibrium, while small particles have to grow fast enough to minimize their Kelvin effect before the concentration of the condensing materials drops to a level making their growth unfeasible. In the observations, some did and some did not, as discussed in the previous section.

Conceptually, gas and particle compositions can be treated as a lumped combination of semi-volatile and low-volatility compounds, which enable us to explain the aerosol dynamics near roadways. Take 405S as an example: The partial pressure of gas phase compounds dropped due to dilution. During the 30–60 m process, the partial pressure of semi-volatile compounds dropped below their vapor pressure and evaporated from particles, while low volatility compounds condensed

since their partial pressure was still above their vapor pressure. For particles in M30C, the gas–particle transport was dominated by evaporation, since volatile compounds account for a larger fraction of those particles. For particles in M30A, condensation of very low volatility material was dominant because those particles did not have much volatile material that could evaporate. The Kelvin effect does not favor condensation of volatile compounds onto small particles. During the 60–90 m process, the 30–60 m trend continued, but the volatile compounds achieved equilibrium between gas and particle phase for the particles larger than 100 nm. For those particles, the gas–particle transport switched to condensation (of low volatility compounds) dominant. The 90–150 m process took twice as long as the previous two, so the aerosol size distribution experienced dramatic change. The partial pressure of low volatility compounds dropped to a level unable to condense on some small particles, so evaporation became dominant for them, while larger particles continued growing by condensation. The size distribution spread out as a result of these dynamics.

Here we introduce a multi-component sectional aerosol dynamic model, simulating only the most important processes in this road-to-ambient process, i.e., dilution and condensation/evaporation. Considering a large number of uncertainties and unknown parameters, we tried to make the model as simple as possible to represent the quintessential parts of this evolution.

3.2. Initiation

Gas and particle composition may contain thousands of different compounds. Representing them explicitly is not feasible and beyond our understanding and the available data. Despite numerous other compounds in exhaust, only organic compound have sufficient abundance to lead to the observed dynamics near roadways (Zhang and Wexler, 2004). The related studies also revealed that organic compounds were the dominant species of particle composition (Kim et al., 2002), which gave rise to our assumption that gas and particle were almost completely composed of organics. Different compounds not only vary in their concentrations, but also vary in their physical properties, most importantly, bulk-phase vapor pressure, P^0, and molar volume, v, which significantly modify their vapor pressure via the Kelvin effect. Thus, we modeled the effective behavior of organic compounds by introducing two different volatility classes, semi-volatile and low volatile. Instead of specifying P^0 and v separately, each class is represented by a single carbon number, CN_s for the semi-volatile and CN_l for the low volatile compounds. Their bulk-phase vapor pressures and molar volumes took the same values as those of alkanes of the same carbon number. The advantages of this approach was that (1) we have a clear reference to evaluate those compounds by comparing to alkanes, whose thermodynamic properties are well understood (Lemmon and Goodwin, 2000); (2) only one variable (the carbon number CN_i) was needed to represent the physical properties, simplifying the model. The disadvantage was that alkanes alone cannot explain growth of nano-sized particles, which favors condensation of compounds with both low volatility and low molar volume (Zhang and Wexler, 2002b). Thus we introduced a third compound, whose vapor pressure is represented by CN_l (same as the low volatility compound) and molar volume by CN_m, which is much smaller than CN_l.

We modeled the same size cuts as measured by the SMPS, extended down to 1 nm and up to 1 μm. The total number of sections after extension was 192. The initial size distributions, i.e., 30 m for 405S and 17 m for 710S, were fitted by superimposition of multiple log-normal modes (Table 3). The modes were chosen consistent with our analysis earlier. The measured number concentration in section i, $N_i(x_0)$, after subtraction of the upwind value in that section, $N_{i,B}$, was distributed into modes so that $N_i(x_0) = \sum_{j=1}^{M} N_i^j(x_0) + N_{i,B}$, where $N_i^j(x_0)$ is the number concentration of particles of mode j in section i and M is the total number of modes. This mode fitting also enabled us to assign number concentrations to particles in the extended sections. Assuming that

Table 3
The initial log-normal fitting parameters and optimized initial molar fractions for semi-volatile compound ($y_{0,semi}$)

	Mode I[a]	Mode II	Mode III	Mode VI	Mode V
405S					
N (cm^{-3})	45,000	50,407	11,419	20,980	19,963
D_{pg} (nm)	3.00	12.50	22.65	32.87	62.30
Ln (std)	0.45	0.44	0.21	0.28	0.58
$y_{0,semi}$	0.01	0.60	0.30	0.80	0.70
	Mode I	Mode II	Mode III		
405W					
N (cm^{-3})	108,770	26,520	45,728		
D_{pg} (nm)	7.30	14.14	27.00		
Ln (std)	0.35	0.34	0.76		
$y_{0,semi}$	0.41	0.48	0.88		
	Mode I	Mode II	Mode III	Mode VI	
710S					
N (cm^{-3})	72,525	26,074	46,548	8306	
D_{pg} (nm)	6.19	10.43	16.67	80.95	
Ln (std)	0.33	0.26	0.68	0.56	
$y_{0,semi}$	0.25	0.67	0.03	0.99	

[a]Denotes the mode below 6 nm and predicted by the model.

particles in the same mode have identical compositions, the composition profile was initiated by specifying the molar fraction of semi-volatile organics in each mode, y_0^j, so that $y_0^j = y_{i,1}^j (i = 1, n)$, where $y_{i,1}^j$ is the molar fraction of semi-volatile organics in mode j and n is the number of size sections. The fraction of low volatility compound, $y_{i,2}^j$, was obtained by mass conservation, $y_{i,2}^j = 1 - y_{i,1}^j$. So particles of the same size may belong to different modes, thus having different compositions and different number concentrations.

3.3. Dilution

Based on the initiation, we derived a simple dilution equation for the particle number and gas-phase compound concentrations as

$$\frac{N_i(x) - N_{i,\mathrm{B}}}{N_i(x - \Delta x) - N_{i,\mathrm{B}}} = \frac{f(x)}{f(x - \Delta x)} = \frac{C_k^{\infty}(x) - C_k^{\mathrm{B}}}{C_k^{\infty}(x - \Delta x) - C_k^{\mathrm{B}}}, \quad (2)$$

where $C_k^{\infty}(x)$ and C_k^{B} are the ambient and background concentration of compound k. Note that Eq. (2) differs from Eq. (1) only in the frame changing from time, t, to distance, x. For a comprehensive air quality model, the dilution function $f(x)$ could be acquired from an atmospheric dispersion model, which is beyond the scope of this study. As mentioned earlier, CO was used as a dilution indicator. Previous studies showed that the CO profile can be described by $C - C_{\mathrm{B}} = (C_{\mathrm{F}} - C_{\mathrm{B}})\exp(A \cdot \Delta x)$ (Zhu et al., 2002b), indicating that $f(x)$ took an exponential form and $f(x)/f(x - \Delta x) = \exp(A \cdot \Delta x)$. In this study A factors were evaluated from f values listed in Table 2.

3.4. Condensation/evaporation

The moving section method was selected to simulate condensation and evaporation. The number concentration in each section remained unchanged and particle size may grow or shrink depending on its mass budget, whose rate of change with respect to time can be

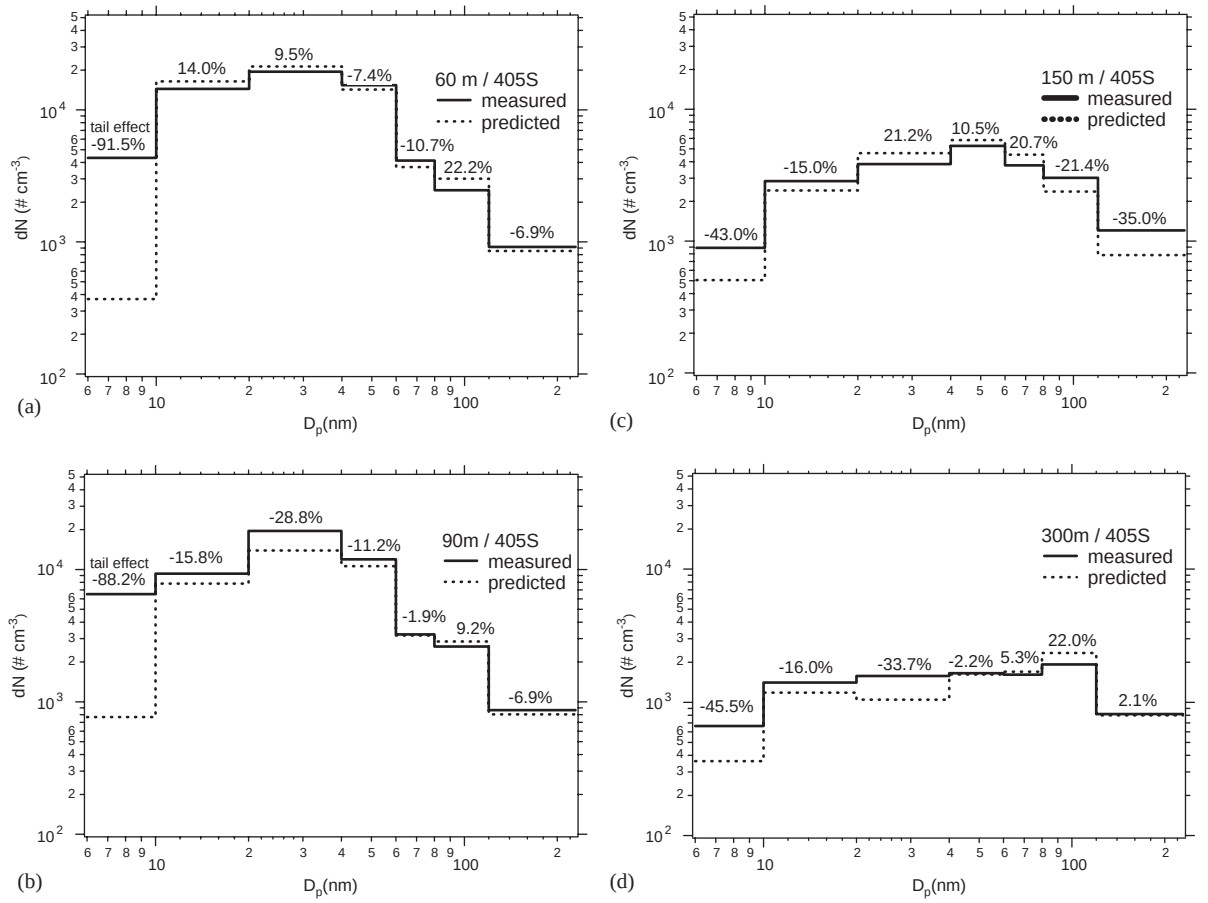

Fig. 2. Simulation of Highway 405 summer study (405S) at (a) 60 m, (b) 90 m, (c) 150 m, and (d) 300 m. The number over each size bin indicates relative difference between measurement and prediction with positive for over-prediction and negative for under-prediction.

expressed as

$$\frac{dm_{i,k}^j}{dt} = \frac{2\pi D_k D_{p,i}^j [C_k^\infty - y_{i,k}^j C_k^0 K_e]}{1 + (8\lambda/\alpha D_{p,i}^j)},$$

where D_k is the diffusivity compound k; α is the accommodation coefficient, taken to be 0.7; λ is air mean free path; K_e is the Kelvin factor (Zhang and Wexler, 2002b); $m_{i,k}^j$ is the mass of compound k in section i of mode j; $y_{i,k}^j$ is the mole fraction of compound k; $D_{p,i}^j$ is the diameter of particle in section i of mode j (Wexler and Seinfeld, 1990; Zhang and Wexler, 2002a).

The Kelvin effect was expressed as $K_e = \exp(4\sigma(14CN+2)/RT\rho_P D_{p,i}^j)$, where σ is the surface tension of the nuclei; ρ_P are the density of the condensing species; R the gas constant, T the temperature; $14CN+2$ represents the molar mass.

According to mass conservation,

$$m_i^j = \frac{\pi (D_{p,i}^j)^3 \rho_p}{6} = \sum_{k=1}^{3} m_{i,k}^j,$$

where m_i^j is single particle mass of mode j in section i. Then $y_{i,k}^j = m_{i,k}^j / m_i^j$ by assuming uniform density for all organic compounds. The change of gas-phase concentration of compound k, C_k^∞, due to condensation/evaporation is

$$\frac{dC_k^\infty}{dt} = N_i^j \frac{dm_{i,k}^j}{dt}.$$

3.5. Parameter identification

Since there was no composition measurement associated with the campaign, the initial gas-phase concentrations and particle compositions were unknown. We employed a minimizer, FFSQP v3.7 (Zhou et al., 1997) to find the best parameters fitting the measurement data.

4. Modeling result and discussion

We choose 7 size bins for model validation against measurement with size cuts at 6, 10, 20, 40, 60, 80, 120

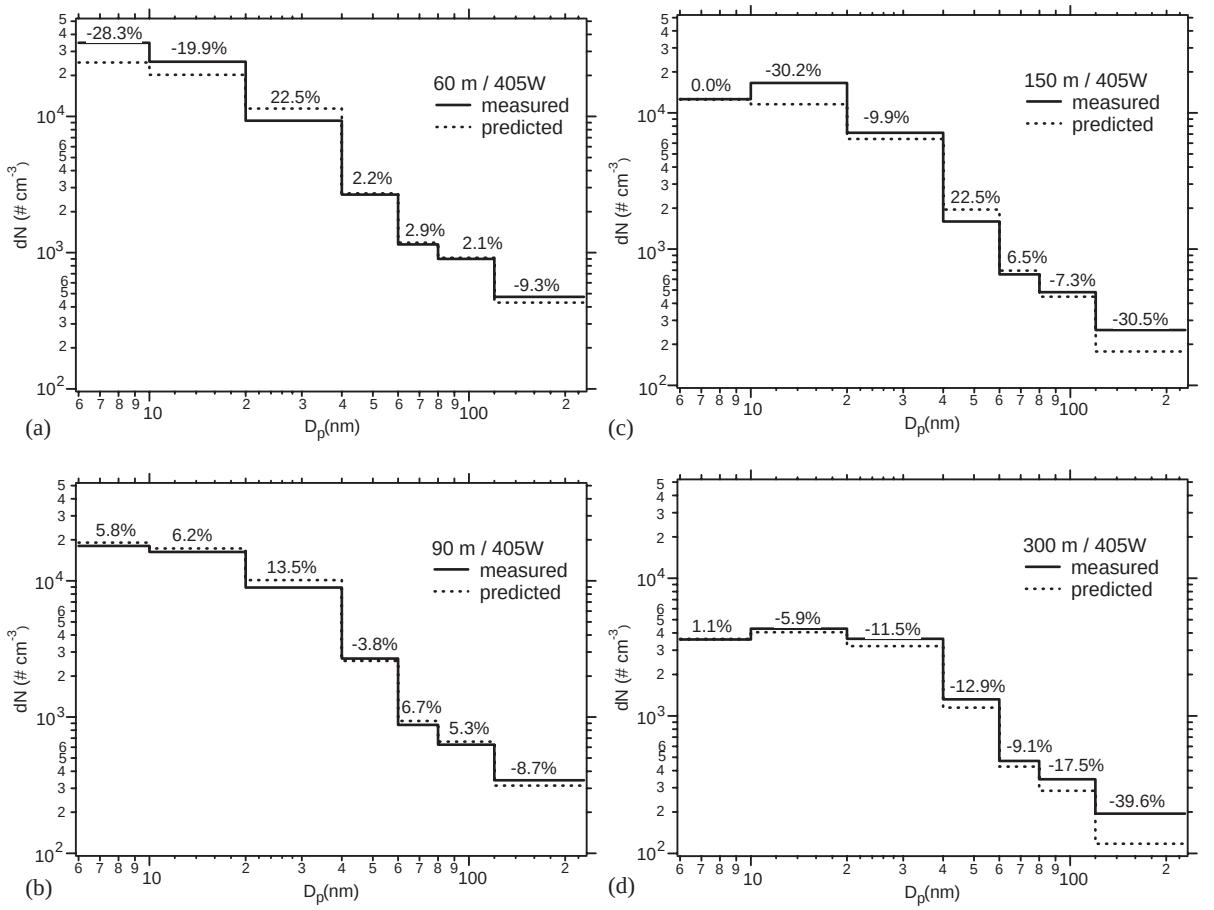

Fig. 3. Simulation of Highway 405 winter study (405W) at (a) 60 m, (b) 90 m, (c) 150 m, and (d) 300 m. The number over each size bin indicates relative difference between measurement and prediction with positive for over-prediction and negative for under-prediction.

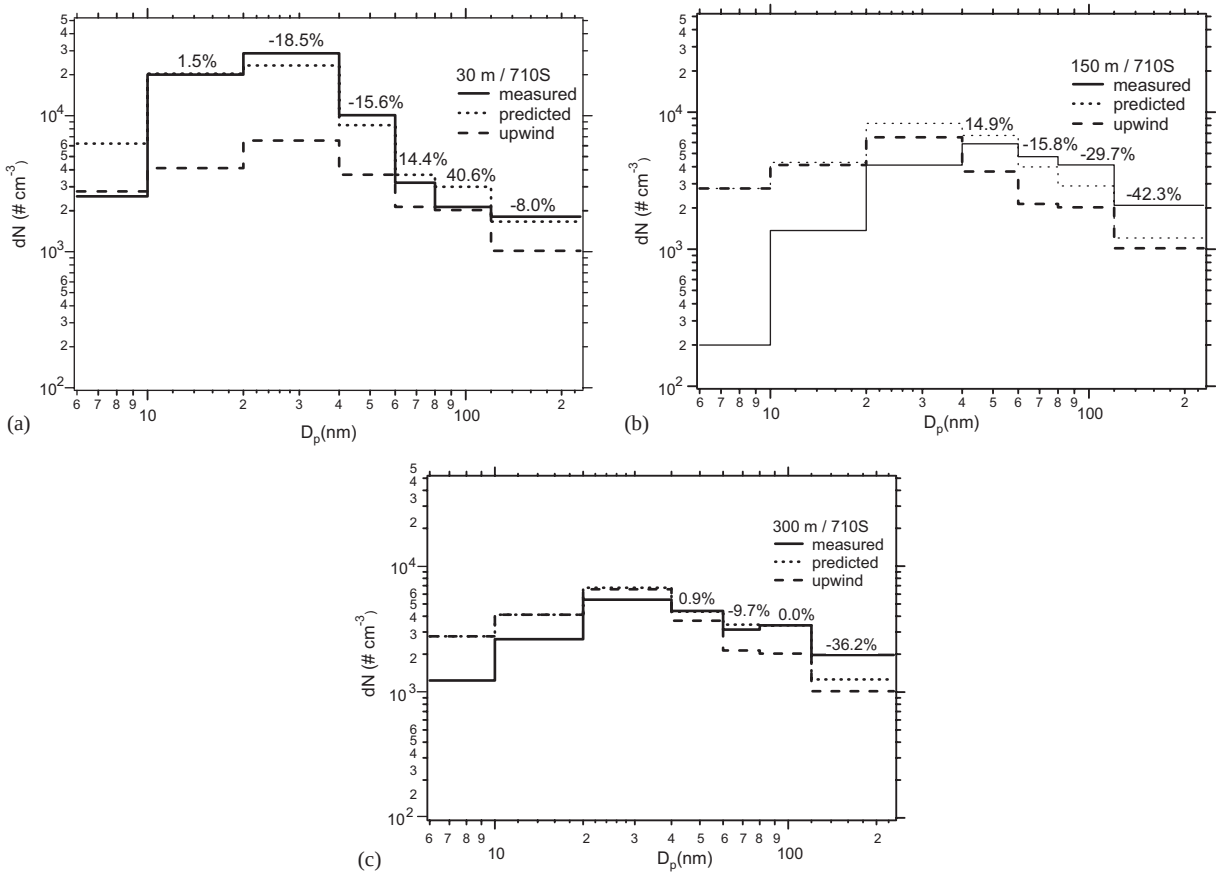

Fig. 4. Simulation of Highway 710 summer study (710S) at (a) 30 m, (b) 150 m, and (c) 300 m. The number over each size bin indicates relative difference between measurement and prediction with positive for over-prediction and negative for under-prediction. Size bins without values indicate measurements below the upwind value in that bin.

and 220 nm. The selection takes into account the modal shapes for all measured size distributions. A uniform size cut for both 405 and 710 facilitated inter-study comparison. Figs. 2–4 illustrate the simulation results for 405S, 405W and 710S. In each figure, model predictions are plotted against measurement data. In Fig. 4, the upwind measurements were also plotted since measured number concentrations were below upwind values for several 710S size bins.

Although the precursor of M60A was below 6 nm at 30 m, we were able to predict a particle reservoir of about 50,000 particles cm^{-3} by keeping track of its growth pattern from 60 to 90 m. We were unable to do the same for M60T and M90T (marked as 'tail effect' in Fig. 1) due to their undeveloped growth pattern and relative large measurement uncertainty. Except for the 6–10 nm range affected by the tail effect, our model closely matched the measurement data for all other size bins at all distances. Our predictions for the 6–10 nm range 405W particles were generally better than 405S, because particles in that range at 60 m shrank from larger sizes at 30 m so we had enough information to track their behavior. Due to reasons discussed earlier, we were only able to compare the model prediction with measurement data at 30, 150 and 300 m for 710S. As shown in Fig. 3, our predictions were very close to upwind levels for size bins where measured values were below upwind values, which indicated upwind particles dominated in those size bins. For other size bins, the modeling results matched measurement data reasonably well given the large variations between passes in Highway 710 measurement.

The relative roles of condensation/evaporation and dilution can be clearly illustrated by turning off the condensation/evaporation operator. Fig. 5 depicts such a comparison for 405S at 150 m. Since the dilution-only model always preserves the initial shape of the size distribution, it led to serious discrepancies from measurement data at later steps of the evolution process, while the dynamic model was able to reproduce the size distributions at all distances even when the relative differences were considered.

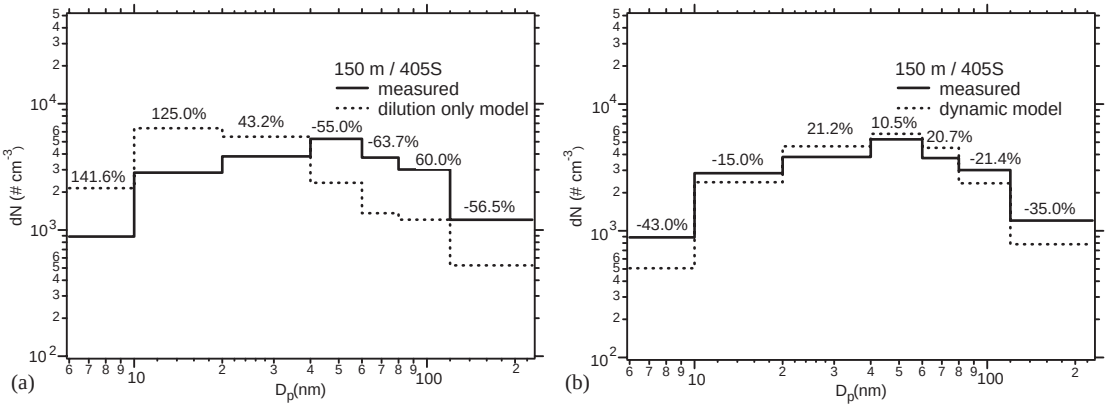

Fig. 5. Comparison between (a) the dilution-only model and (b) the dynamic model for Highway 405 summer study (405S) at 150 m.

Aerosol dynamics is driven toward gas–particle equilibrium. Particle compositions could change dramatically in this process as components adapt to decreasing gas-phase concentration due to dilution. Thus, evolution of number distribution is also an evolution of compositions. The optimal CN_s and CN_l were 21 and 24, respectively. Those numbers fall into the range where the largest fuel molecules and smallest lubrication oil molecules reside (Sakurai et al., 2002). CN_m varied from 1 to 3 for different studies. Since some other lumping methods may also match the measured distribution, we have limited confidence in our lumped gas and particle composition predictions. Nevertheless, the effective amount of materials condensed and evaporated was much more certain since it can be validated from size distribution profiles. Measurement of gas and particle composition at various downwind distances would provide a much more solid foundation for composition modeling.

5. Conclusion

In this study, we first analyzed the 'road-to-ambient' datasets measured near Highway 405 and 710 in Los Angeles, CA. Our analysis showed that (a) seasonal effects were significant with winters generally less dynamic than summers, and (b) a large number of sub-6 nm particles emitted from freeways may grow above 10 nm around 30–90 m downwind. Afterwards, some shrink back to sub-10 nm and some continue growing to above the 100 nm range. This phenomenon implies that people who live within 90 m of roadways are exposed to particles that others are not.

In addition, we successfully simulated the evolution using a multi-component aerosol dynamic model. The model was fitted to measurements to identify the physico-chemical properties of the volatile species. Compared with a dilution-only model, it is better able to capture the aerosol dynamics during this evolution process. The good agreement between the modeled and measured number size distributions at various downwind distances confirmed our analysis of aerosol dynamics in the 'road-to-ambient' evolution process, i.e., dilution and condensation/evaporation are the dominant mechanisms, while the effects of coagulation and deposition are minor. The fitted parameters indicted that the lumped, alkane-equivalent carbon number for condensing organic vapors are around 21–24.

Acknowledgements

KMZ and ASW would like to thank EPRI and NSF (Grant # CHE-0089136) for supporting analysis and modeling of the data. YZ, WCH and CS would like to acknowledge support from the Southern California Particle Center and Supersite: US Environmental Protection Agency Grant Number R82735201, California Air Resources Board contract number 98-316, and the Southern California Environmental Health Center, National Institute of Environmental Health Sciences (NIEHS) Grant # 5 P30 ES07048-07.

References

Hoek, G., Brunekreef, B., Goldbohm, S., Fischer, P., van den Brandt, P.A., 2002. Association between mortality and indicators of traffic-related air pollution in the Netherlands: a cohort study. Lancet 360 (9341), 1203–1209.

Kim, S., Shen, S., Sioutas, C., Zhu, Y.F., Hinds, W.C., 2002. Size distribution and diurnal and seasonal trends of ultrafine particles in source and receptor sites of the Los Angeles basin. Journal of the Air and Waste Management Association 52 (3), 297–307.

Kunzli, N., McConnell, R., Bates, D., Bastain, T., Hricko, A., Lurmann, F., Avol, E., Gilliland, F., Peters, J., 2003.

Breathless in Los Angeles: the exhausting search for clean air. American Journal of Public Health 93 (9), 1494–1499.

Lemmon, E.W., Goodwin, A.R.H., 2000. Critical properties and vapor pressure equation for alkanes C_nH_{2n+2}: normal alkanes with $n \leqslant 36$ and isomers for $n=4$ through $n=9$. Journal of Physical and Chemical Reference Data 29 (1), 1–39.

Sakurai, H., Tobias, H.J., Park, K., Zarling, D., Docherty, S., Kittelson, D.B., McMurry, P.H., Ziemann, P.J., 2002. On-line measurements of diesel nanoparticle composition and volatility. Atmospheric Environment 37 (9–10), 1199–1210.

SCAQMD, 2000. Multiple Air Toxics Exposure Study in the South Coast Air Basin: MATES-II (Final Report), March 2000 (Chapter 5).

STPP, 2003. Clearing the Air. A Report of the Surface Transportation Policy Project (STPP).

Wexler, A.S., Seinfeld, J.H., 1990. The distribution of ammonium salts among a size and composition dispersed aerosol. Atmospheric Environment 25A, 1231–1246.

Zhang, K.M., Wexler, A.S., 2002a. Modeling the number distributions of urban and regional aerosols: theoretical foundations. Atmospheric Environment 36 (11), 1863–1874.

Zhang, K.M., Wexler, A.S., 2002b. A hypothesis for growth of fresh atmospheric nuclei. Journal of Geophysical Research—Atmospheres 107 (D21) Art. No. 4577.

Zhang, K.M., Wexler, A.S., 2004. Evolution of particle number distribution near roadways. Part I: analysis of aerosol dynamics and its implications for engine emission measurement. Atmospheric Environment, this issue, doi:10.1016/j.atmosenv.2004.06.043.

Zhou, J.L., Tits, A.L., Lawrence, C.T., 1997. User's guide for FFSQP Version 3.7: A FORTRAN code for solving constrained nonlinear (Minimax) optimization problems, generating iterates satisfying all inequality and linear constraints. Institute for Systems Research and Electrical Engineering Department, University of Maryland, College Park, MD 20742.

Zhu, Y., Hinds, W.C., Kim, S., Sioutas, C., 2002a. Concentration and size distribution of ultrafine particles near a major highway. Journal of the Air and Waste Management Association 52, 1032–1042.

Zhu, Y., Hinds, W.C., Kim, S., Shen, S., Sioutas, C., 2002b. Study of ultrafine particles near a major highway with heavy-duty diesel traffic. Atmospheric Environment 36 (27), 4323–4335.

Zhu, Y., Hinds, W.C., Kim, S., Shen, S., Sioutas, C., 2004. Seasonal trends of concentration and size distribution of ultrafine particles near major highways in Los Angeles. Aerosol Science and Technology 38 (Suppl. 1), 5–13.